Comparative susceptibility of Old World and New World bat cell lines to Zika virus: Insights into viral replication and inflammatory responses

Alexander J. Brown[1‡] and Anna C. Fagre[2‡*], Julianna Gilson[1], Jennifer Horton[1], Ricardo Rivero[1], Mahsan Karimi[1], Emily Speranza[3], Michael Letko[1], Stephanie N. Seifert[1*]
[‡]These authors contributed equally, [*]co-communicating authors

[1]Paul G. Allen School for Global Health; Washington State University, Pullman, WA
[2]Department of Microbiology, Immunology, and Pathology; Colorado State University, Fort Collins, CO
[3]Florida Research and Innovation Center; Cleveland Clinic Lerner Research Institute, Port St. Lucie, FL

ABSTRACT

Background

From the first isolation of Zika virus (ZIKV) in Uganda in 1947, ZIKV had primarily been associated with sporadic human cases in Africa and Asia until ZIKV emerged as an epidemic in the Americas in 2015. As ZIKV spread into new geographic regions, it now has the potential to interact with many novel potential host species whose susceptibility to the virus has yet to be determined. Bats, with their ability to fly and live in or near human structures, are plausible ZIKV reservoirs. However, their competence as hosts for ZIKV remains unresolved. In this study, we investigate the immune response of Old World and New World bats to ZIKV infection *in vitro*.

Results

We demonstrate that Egyptian Rousette bat (*Rousettus aegyptiacus;* Old World) cells are susceptible to ZIKV, while we observed little to no ZIKV replication in Jamaican fruit bat (*Artibeus jamaicensis*) cells. Notably, both the Asian and African ZIKV lineages elicited a strong proinflammatory response in the *R. aegyptiacus* cell line including upregulation of *IL6*, *CXCL8*, and *CCL5*. These data contrast with the dampened inflammatory response detected in these bats to other viruses.

Conclusions

The findings reveal that R06E cells derived from Egyptian Rousette bats exhibit robust proinflammatory and antiviral responses upon Zika virus (ZIKV) infection, characterized by significant upregulation of proinflammatory cytokines. This suggests that while these cells support productive ZIKV replication, they also mount a strong immune response, challenging the notion of these bats as immune-tolerant reservoirs and indicating a more complex interaction with the virus.

INTRODUCTION

Zika virus (ZIKV), primarily transmitted by the *Aedes aegypti* mosquito, is a global health concern due to its association with congenital microcephaly and Guillain-Barre syndrome(1,2). Since the virus was first isolated in Uganda in 1947, ZIKV had primarily been associated with sporadic human cases in Africa(3,4). However, in the early 2000s, the Asiatic lineage began to emerge in larger outbreaks in the Pacific Islands before emerging as an epidemic in the Americas 2015(5)(6). The African lineage of ZIKV results in higher pathogenesis than the Asian lineage, including elevated levels of inflammatory cytokines (e.g. interleukin 6) and tumor necrosis factor(7–9). The African ZIKV lineage is more frequently associated with the Guillain-Barre syndrome, a neurological manifestation of ZIKV, in infected adults(9,10). While considered less virulent, the Asian lineage is associated with higher incidence of congenital microcephaly(10).

Mathematical modeling of ZIKV outbreaks indicates a sylvatic transmission cycle involving wildlife hosts in addition to human hosts(11,12). While both Old World and New World nonhuman primates (NHPs) are susceptible to ZIKV(13)(14), outbreaks of Zika virus disease in South America have occurred in areas without detection of ZIKV in NHPs(11). Bats have been posited as an alternative sylvatic reservoir for ZIKV as several species roost in or near human dwellings and there is evidence of bat exposures to arboviruses(15–18) including ZIKV(4). However, data on the circulation, pathology, and susceptibility of bats to ZIKV are unclear, particularly in the Americas where ZIKV has only recently been introduced.

Early experimental work examining susceptibility of Ugandan bat species to ZIKV suggests they develop low levels of viremia in the absence of clinical disease. Inoculation of an Angolan fruit bat (*Myonycteris angolensis*) indicated a low level of viremia up to 6 days post-infection (DPI)(16). In another study, low levels of viremia and seroconversion were detected in straw-coloured fruit bats (*Eidolon helvum*) and Egyptian rousette bats (*Rousettus aegyptiacus*, ERBs) intraperitoneally inoculated with ZIKV(17). In a subsequent study, ZIKV-reactive antibodies were detected in both bat taxa by a hemagglutination inhibition assay(17). Detection of ZIKV subgenomic flavivirus RNA (sfRNA) in splenic samples of Ugandan fruit bats including straw-coloured fruit bats, Ethiopian epauletted (*Epomophorus labiatus*) fruit bats and ERBs suggests previous ZIKV infection, though questions remain surrounding the relationship of sfRNA to the timing of viral infection and/or clearance (4). Serum from these bats did not contain neutralizing antibodies against ZIKV or other flaviviruses(19). Experimental inoculation of insectivorous bats including Angolan free-tailed bats (*Mops condylurus*) with ZIKV did not result in viremia, but serosurveillance data indicates a high seroprevalence for ZIKV exposure in both the Angolan and the little free-tailed bat (*Mops* [*Chaerephon*] *pumilus*)(16,17,20). Thus, data on susceptibility of Old World bat species to ZIKV is limited and largely inconclusive.

127 Surveillance studies examining neotropical bats and other small mammals for evidence
128 of ZIKV infection have increased since the 2015 introduction of the Asian lineage of
129 ZIKV. Viral RNA has been detected in common vampire bats (*Desmodus rotundus*) and
130 Jamaican fruit bats (*Artibeus jamaicensis*, JFBs) in Mexico(21,22), though a more
131 recent study screening 162 bats across 23 species found no evidence of ZIKV infection
132 by quantitative reverse-transcription polymerase chain reaction(23). A short sequence
133 fragment of the ZIKV NS5 gene, associated with the flat-faced fruit bat (*Artibeus*
134 *planirostris*) from Grenada, West Indies, was deposited in GenBank (Accession
135 #MH255606) in 2018, though this sequence has not been linked to a peer-reviewed
136 publication. Large surveys across Central and South America, including Brazil, French
137 Guiana, Peru, and Costa Rica, have not detected ZIKV nucleic acids in bats(23–25).
138
139 Studies with experimental challenge *in vivo* also suggest limited susceptibility of
140 neotropical bats to ZIKV. Inoculation of bats in the genus *Artibeus* resulted in minimal
141 pathology with variable detection of viral RNA in brain, urine, and saliva but viremia was
142 not observed(26). A follow-up study reported detection of ZIKV subgenomic flavivirus
143 RNA (sfRNA) in blood and multiple organs of JFBs up to six weeks post-inoculation with
144 three different ZIKV strains(4). Inoculation of the great fruit-eating bat (*Artibeus literatus*)
145 with an Asian lineage ZIKV isolate did not result in detectable viremia or the production
146 of neutralizing antibodies, though ZIKV RNA was detected in two of nine inoculated
147 bats(24). While these findings suggest that New World bats may be susceptible to ZIKV,
148 evidence that they develop viremia sufficient to contribute to viral transmission is
149 lacking.
150
151 African bats have co-existed with ZIKV over an extended period, whereas bats in the
152 Americas have only been exposed for about a decade following introduction of the
153 Asian ZIKV lineage. Given their synanthropic behavior and prominence at the human-
154 animal interface, bats are plausible amplifying hosts ecologically capable of contributing
155 to ZIKV transmission and spread. However, a fundamental question remains: Are bats
156 susceptible to ZIKV infection? Susceptibility requires both viral entry into host cells and
157 evasion of innate immune defenses. Here, we investigate the *in vitro* susceptibility and
158 transcriptional responses of bat cells derived from ERBs (Old World) and JFBs (New
159 World) following infection with African and Asian ZIKV lineages.
160
161 **RESULTS**
162
163 **Comparative growth curves**
164 We first determined the susceptibility of two immortalized cell lines derived from the
165 Egyptian rousette bat, *Rousettus aegyptiacus* (R06E cells), and the Jamaican fruit bat,
166 *Artibeus jamaicensis* (Aji cells) to ZIKV isolates representing the African (ZIKV/MR766)
167 or Asian (ZIKV/PRVABC59) lineages by performing comparative growth curves. While
168 both ZIKV isolates replicated in the R06E cells (Fig 1A), neither strain replicated in the
169 Aji cells (Fig 1B). A small reduction in titers for ZIKV/MR766 at 24 hours post-inoculation
170 (HPI) and subsequent return to baseline may indicate binding of virus to Aji cells without

171 productive internalization or replication.
172

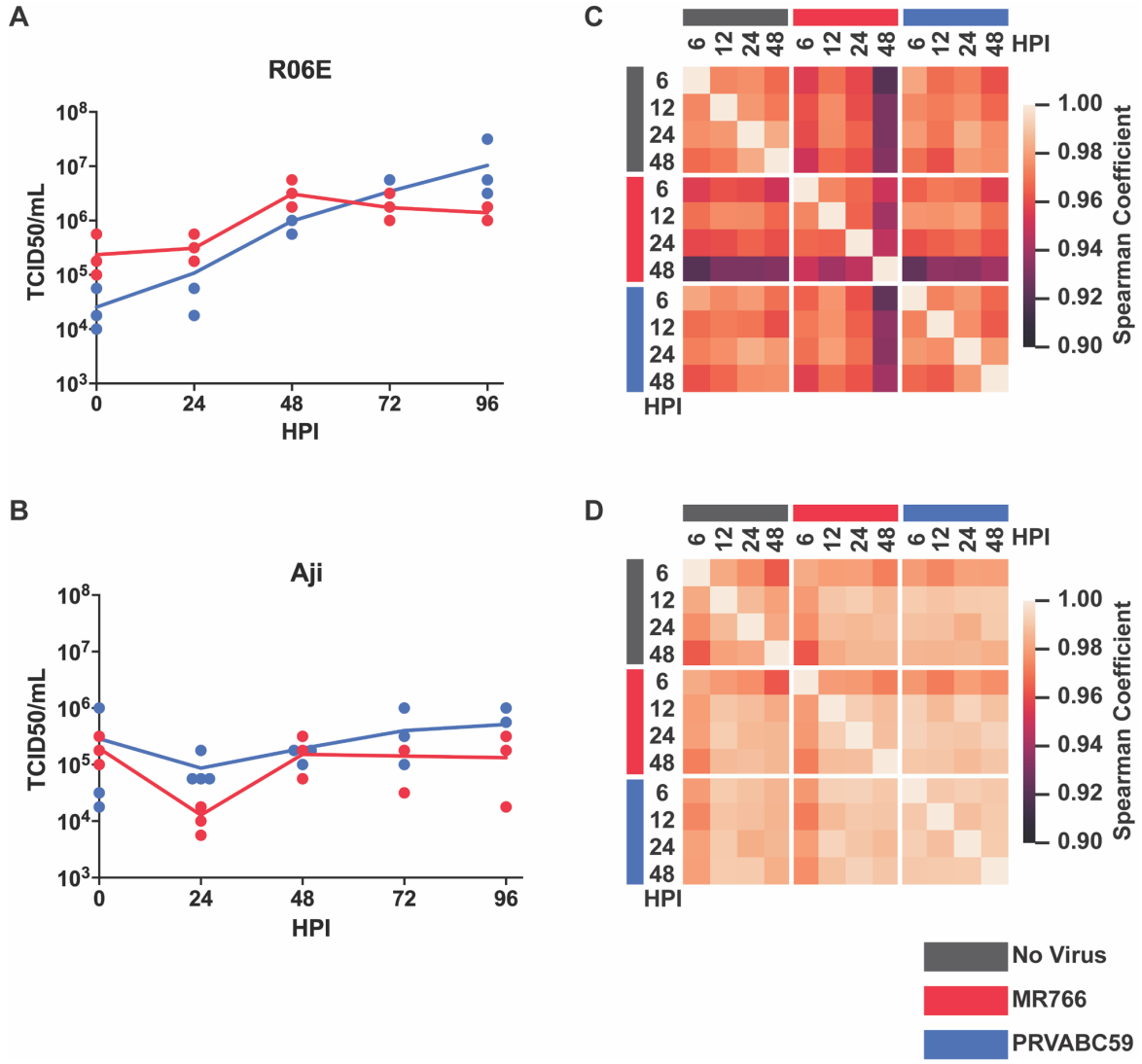

Figure 1. Comparative growth curves and normalized gene counts for Egyptian rousette bat (R06E) and Jamaican fruit bat (Aji) cell lines with African (MR766) and Asian (PRVABC59) ZIKV isolates. (**A**) Growth curves of ZIKV/MR766 and PRVABC59 isolates in R06E cells over 96 hours post-inoculation (HPI). (**B**) Aji cells did not support cumulative viral growth over 96 HPI for either ZIKV isolate. Dots represent replicates; the line represents the median. (**C**) Spearman correlation analysis of normalized gene counts in R06E cells showed high similarity among samples, with a minimum coefficient of 0.9201. (**D**) Aji samples exhibited even higher similarity, with a minimum Spearman coefficient of 0.9625. The colored bar legend in the bottom right corresponds to all panels of the figure.

173
174
175
176

Transcriptomic response to ZIKV infection *in vitro*

To assess the transcriptional responses of R06E and Aji cells to ZIKV infection, we performed total RNA sequencing on samples from both cell lines, either uninfected or infected with an African (ZIKV/MR766) or Asian (ZIKV/PRVABC59) lineage isolate at 6, 12, 24, and 48 HPI. After quality control and filtering (see Materials and Methods), gene counts were successfully obtained, normalized, and corrected for batch effects.

Spearman correlation analysis of gene counts revealed distinct patterns of similarity between treatment groups. In R06E cells, treatment groups were generally more similar to themselves than to other groups, though all samples remained highly correlated, with the lowest Spearman coefficient at 0.9201 (Fig 1C). Notably, within-group similarity decreased over time, even in untreated samples highlighting the importance of comparing the ZIKV experimental group against the negative control group at each time point rather than to 0 HPI. In contrast, Aji cells exhibited high correlation across all conditions, with the lowest Spearman coefficient at 0.9625 (Fig 1D), indicating minimal transcriptomic divergence between infected and uninfected states.

Principal Component Analysis (PCA) further supported these observations. In Aji cells, time was the dominant principal component, accounting for 98.41% and 98.44% of the variance in ZIKV/MR766- and ZIKV/PRVABC59-treated samples, respectively (Supplemental Figure 1C, 1D). Conversely, in R06E cells, time was not the primary driver of variability, contributing only 12.11% and 9.96% to the variance in MR766- and PRVABC59-treated samples, respectively (Supplemental Figure 1A, 1B).

Together, these findings suggest that R06E cells were successfully infected by ZIKV, as indicated by transcriptomic divergence following treatment. In contrast, the persistent similarity among Aji samples across time points and treatment conditions suggests that viral replication was effectively blocked in these cells, preventing downstream transcriptional changes associated with infection.

<u>Gene set enrichment analysis reveals strong anti-viral response in Egyptian rousette cells to ZIKV infection</u>

To characterize the global transcriptional response of R06E cells to ZIKV infection, we performed gene set enrichment analysis (GSEA) (see Materials and Methods). The most significant enrichment was observed at 6 HPI, with upregulated gene sets shared between both ZIKV/MR766 and PRVABC59 isolates. These included pathways involved in immune responses, such as “viral protein interaction with cytokine and cytokine receptor,” “malaria,” “rheumatoid arthritis,” and “toll-like receptor signaling pathway” (Fig. 2A, B). Notably, no gene sets were significantly downregulated at this timepoint.

217

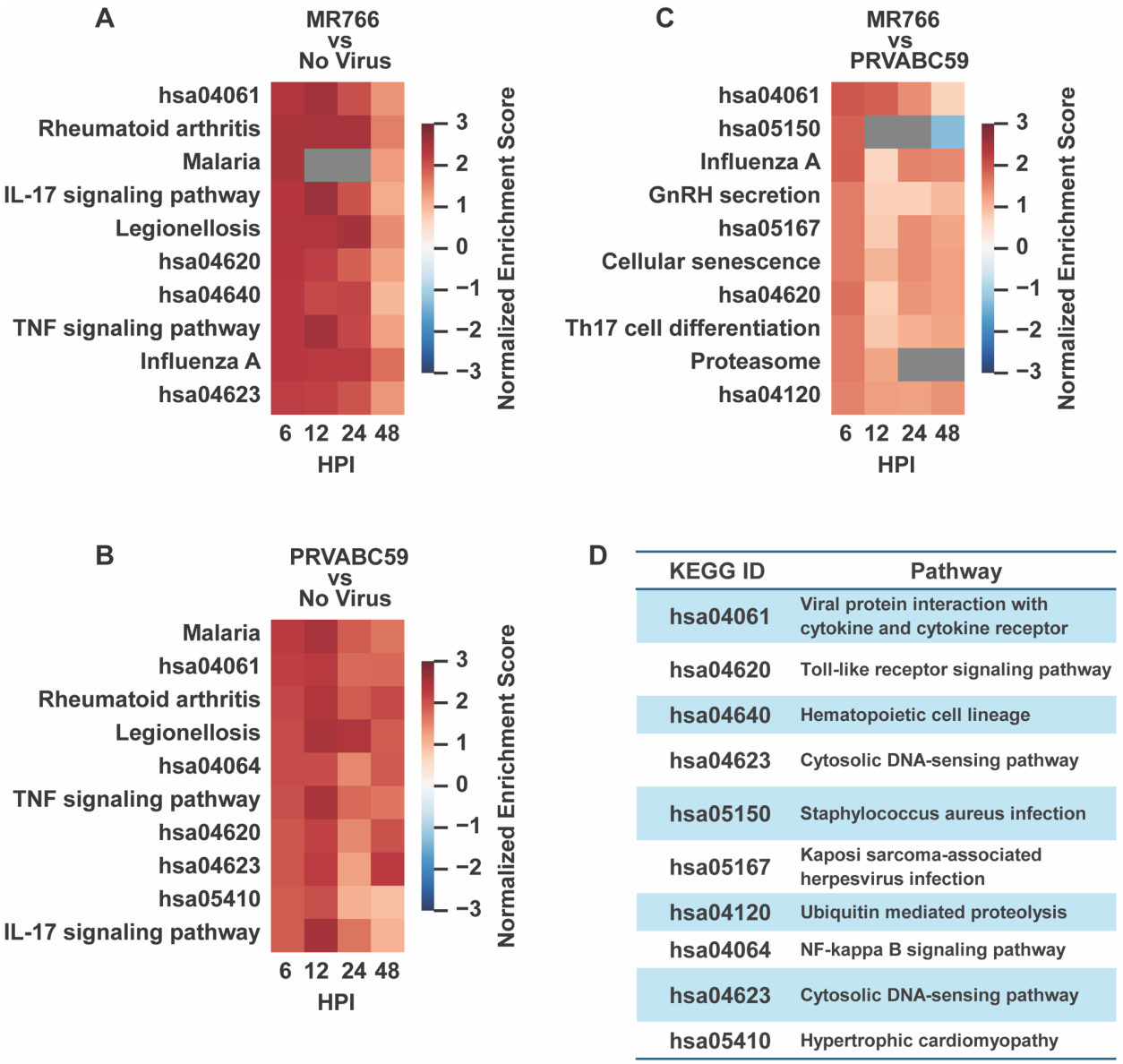

KEGG ID	Pathway
hsa04061	Viral protein interaction with cytokine and cytokine receptor
hsa04620	Toll-like receptor signaling pathway
hsa04640	Hematopoietic cell lineage
hsa04623	Cytosolic DNA-sensing pathway
hsa05150	Staphylococcus aureus infection
hsa05167	Kaposi sarcoma-associated herpesvirus infection
hsa04120	Ubiquitin mediated proteolysis
hsa04064	NF-kappa B signaling pathway
hsa04623	Cytosolic DNA-sensing pathway
hsa05410	Hypertrophic cardiomyopathy

Figure 2. Gene set enrichment analysis (GSEA) of R06E cells following ZIKV infection. Genes were ranked by $\log_2$ fold change and p-value (see Materials and Methods), and GSEA was performed using KEGG_2021_Human gene sets. Upregulated and downregulated genes were analyzed separately, with no significant downregulated gene sets observed. The top 10 upregulated gene sets at 6 HPI (FDR < 0.1) are shown, along with normalized enrichment scores (NES) across all timepoints. Grey boxes indicate timepoints where no NES was calculated due to a lack of upregulated genes in the gene set. (**A**) ZIKV/MR766-infected R06E cells showed enrichment of antiviral and pro-inflammatory gene sets. (**B**) ZIKV/PRVABC59-infected R06E cells displayed a similar enrichment pattern. (**C**) Direct comparison of ZIKV/MR766 vs. PRVABC59 in R06E cells revealed reduced enrichment of the same gene sets. (**D**) KEGG ID to associated pathway.

To assess strain-specific differences, we compared gene expression changes directly between ZIKV/MR766 and PRVABC59-infected R06E cells. The enrichment magnitude for all gene sets was markedly reduced (Fig. 2C), though pathways associated with viral infection remained detectable. Among these, “viral protein interaction with cytokine and cytokine receptor” was the most consistently enriched across timepoints, suggesting that the African ZIKV isolate (ZIKV/MR766) elicits a stronger and earlier transcriptional response than the Asian ZIKV lineage isolate (ZIKV/PRVABC59).

To further validate our findings in Aji cells, we performed GSEA on these samples as well. However, nearly all enriched gene sets had false discovery rates (FDR) exceeding 0.1, rendering them statistically insignificant. The only significant gene sets for ZIKV/PRVABC59-infected Aji cells at 6 HPI included “ribosome,” “Parkinson disease,” and “valine, leucine, and isoleucine degradation,” which lack clear biological relevance to viral infection. Additionally, Spearman correlation analysis (Fig. 1D) indicated that untreated Aji samples at 6 HPI were highly dissimilar from other Aji samples, suggesting a potential technical artifact influencing gene counts at this timepoint.

Overall, these results reinforce that R06E cells support ZIKV replication and mount a robust immune response, while Aji cells do not exhibit a clear transcriptional signature of infection. Consequently, Aji samples were excluded from subsequent analyses.

Gene ontology enrichment analysis (GOEA) corroborates GSEA results

The GSEA results generally correspond to what we would expect based on ZIKV literature, but we recognize using human gene sets for the GSEA could create some species-specific bias or miss species-specific effects when considering responses in bats. To corroborate our findings with an orthogonal approach, we performed gene ontology enrichment analysis (GOEA) using differentially expressed genes (DEGs) (see Materials and Methods). Many enriched GO terms were redundant, so we grouped them using GO slim categories and selected the most significant term within each group for clarity (Supplemental Figure 2, Supplemental Table 1).

The top 10 statistically significant, enriched GO terms for each viral contrast are shown in Fig. 3. ZIKV/MR766-infected R06E cells exhibited strong enrichment for immune-related processes, including “defense response to symbiont,” “immune response,” and “cell surface signaling pathway” (Fig. 3A). ZIKV/PRVABC59-infected cells displayed similar enrichment patterns, with top terms including “defense response,” “cytokine-mediated signaling pathway,” and “neutrophil chemotaxis” (Fig. 3B). These results align with the previously identified enriched gene sets, such as “Influenza A” and “viral protein

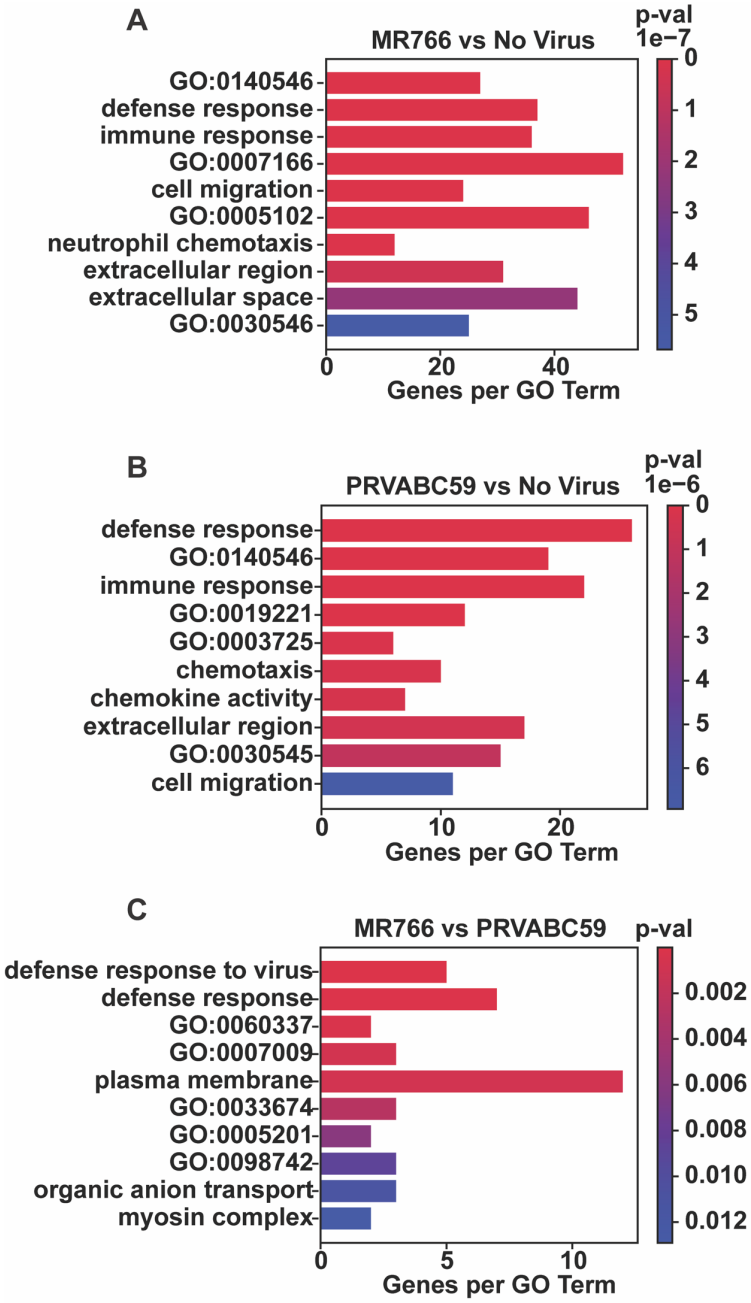

D

GO ID	GO Term
GO:0140546	defense response to symbiont
GO:0007166	cell surface receptor signaling pathway
GO:0005102	signaling receptor binding
GO:0030546	signaling receptor activator activity
GO:0019221	cytokine-mediated signaling pathway
GO:0003725	double-stranded RNA binding
GO:0030545	signaling receptor regulator activity
GO:0060337	type I interferon-mediated signaling pathway
GO:0007009	plasma membrane organization
GO:0033674	positive regulation of kinase activity
GO:0005201	extracellular matrix structural constituent
GO:0098742	cell-cell adhesion via plasma-membrane adhesion molecules

Figure 3. Gene ontology enrichment analysis (GOEA) of differentially expressed genes (DEGs) in ZIKV-infected R06E cells. GOEA was performed on DEGs from each viral contrast to identify enriched GO terms. To improve interpretation, terms were grouped by GO slim categories, with the most significant term representing each group. The top 10 enriched GO terms are shown, color-coded by unadjusted p-values. (**A**) ZIKV/MR766-infected R06E cells showed strong enrichment for antiviral pathways. (**B**) ZIKV/PRVABC59-infected cells displayed a similar enrichment pattern. (**C**) Direct comparison of ZIKV/MR766 vs. PRVABC59 revealed reduced enrichment, with lower significance and fewer genes contributing to each GO term. (**D**) GO identification numbers to functional categories.

interaction with cytokine and cytokine receptor" (Fig. 2A, B). When directly comparing R06E transcriptional response to infection with ZIKV/MR766 versus ZIKV/PRVABC59, GOEA revealed significant differences in terms such as "defense response to virus" and "type I interferon-mediated signaling pathway" (Fig. 3C). However, the statistical significance and gene support for these terms were reduced, mirroring the decrease in normalized enrichment scores observed in GSEA (Fig. 2C). Together, GOEA and GSEA results indicate that both ZIKV isolates induce similar immune responses in R06E cells, with ZIKV/MR766 eliciting a stronger antiviral and pro-inflammatory response.

DEG clustering and GOEA suggest subtle differences in ZIKV/MR766 and ZIKV/PRVABC59-induced responses

The previous analyses indicate that ZIKV/MR766 and PRVABC59 elicit similar antiviral and pro-inflammatory responses in R06E cells. However, GSEA relies on predefined gene sets, and our GOEA did not distinguish between up- and downregulated genes, though most DEGs were upregulated. To further explore transcriptional responses, we clustered DEGs based on similar expression profiles across timepoints and analyzed their functional enrichment.

Since previous analyses showed strong similarity between ZIKV/MR766- and PRVABC59-infected R06E cells, we focused on this comparison to highlight isolate-specific differences in the transcriptional response. DEG expression clustering identified three major groups. Group 10 exhibited a general increase in expression across all timepoints (Fig. 4A) and was enriched for antiviral GO terms such as "defense response to virus" and "type I interferon-mediated signaling pathway (GO:0060337)" (Fig. 4B), driven by interferon-stimulated genes including *OAS3*, *MX2*, *IFIT3*, *IFI6*, and *DDX58*. Additionally, ZIKV/MR766 elicited a stronger response at 6 HPI than PRVABC59, consistent with GSEA findings (Fig. 2C).

In contrast, Groups 5 and 8 showed more distinct expression patterns, with ZIKV/MR766 eliciting stronger responses at 6 and 48 HPI, but similar levels at 12 and 24 HPI (Fig. 4C, E). These groups were enriched for less intuitive GO terms, including "GTPase activator activity" (Fig. 4D) and "transmembrane receptor protein tyrosine kinase activity (GO:0004714)" (Fig. 4F). Many flaviviruses, including ZIKV, enter host cells through clathrin-mediated endocytosis, a process that depends heavily on small GTPases(27) and tyrosine kinase receptors to facilitate viral entry, replication, and egress(28). Consequently, while the exact roles of groups 5 and 8 in viral response remain unclear, these findings suggest additional biological processes may contribute to ZIKV infection dynamics.

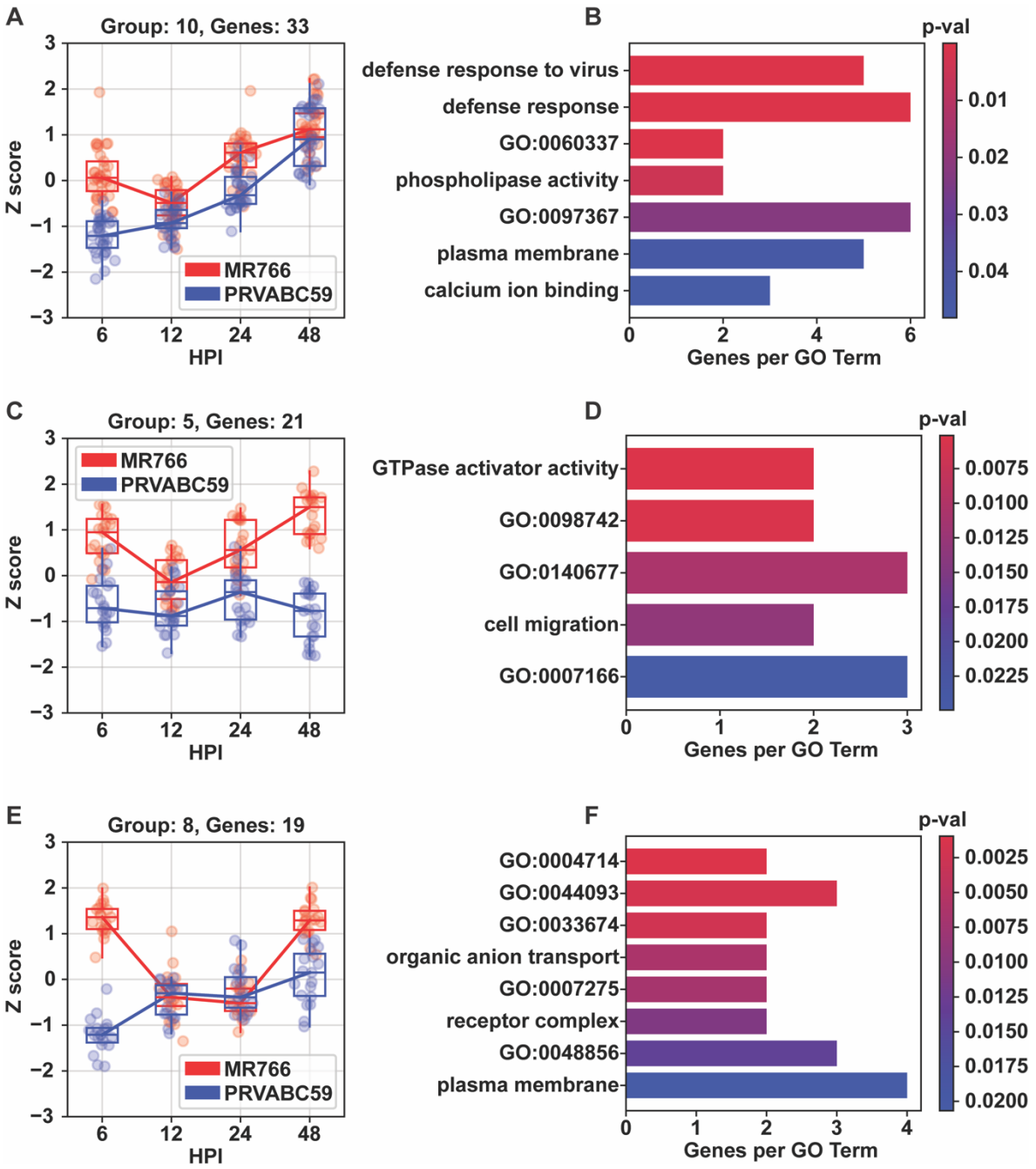

Figure 4. Clustering of differentially expressed genes (DEGs) in R06E cells infected with African (MR766) and Asian (PRVABC59) ZIKV isolates. Gene counts were converted to Z-scores and grouped by similar expression patterns. Boxes represent quartiles and median values, while dots indicate mean relative abundance per gene. (**A**) Group 10 genes increased in expression over time, with larger divergence at 6 HPI. (**B**) GOEA revealed enrichment for defense response terms. (**C, E**) Groups 5 and 8 showed increased expression at 6 and 48 HPI in MR766-infected cells. (**D, F**) However, some enriched GO terms were not clearly linked to antiviral activity. For bars labelled with GO IDs, see Supplemental Table 1 for full GO terms.

300

301 ***CCL20, CCL5*, *CXCL8*, and *IL6* may play a role in the differential response**
302 **between ZIKV/MR766 and PRVABC59 infected R06E cells**
303 Given that the "viral protein interaction with cytokine and cytokine receptor" gene set
304 was more enriched than any other in the ZIKV/MR766 vs PRVABC59 contrast (Figure
305 2C), we further examined its gene composition, focusing on upregulated genes. GSEA
306 at 6 HPI revealed that the enrichment was primarily driven by *CCL20*, *CCL5*, *CXCL8*,
307 and *IL6*, which ranked among the most upregulated genes in the set (Figure 5A).
308 Heatmap analysis and manual inspection confirmed that *CCL20*, *CCL5*, *CXCL8*, and
309 *IL6* exhibited some of the highest $\log_2$ fold changes within the set at 6 HPI, although
310 they do generally decrease over time (Figure 5B).
311
312 To better understand the relationship between these genes, we used the STRING
313 database (29) to generate a protein-protein interaction (PPI) network of the analyzed
314 genes in the set (Fig 5C; see Materials and Methods). We observed that *CCL5*, *CXCL8*,
315 and *IL6* emerged as hub genes having the highest number of interactions with other
316 proteins (16 interactions) in the network (average of 10.63 interactions). Hub genes
317 likely perform a critical role in modulating the entire network or performing other
318 biological processes.
319
320
321
322
323
324

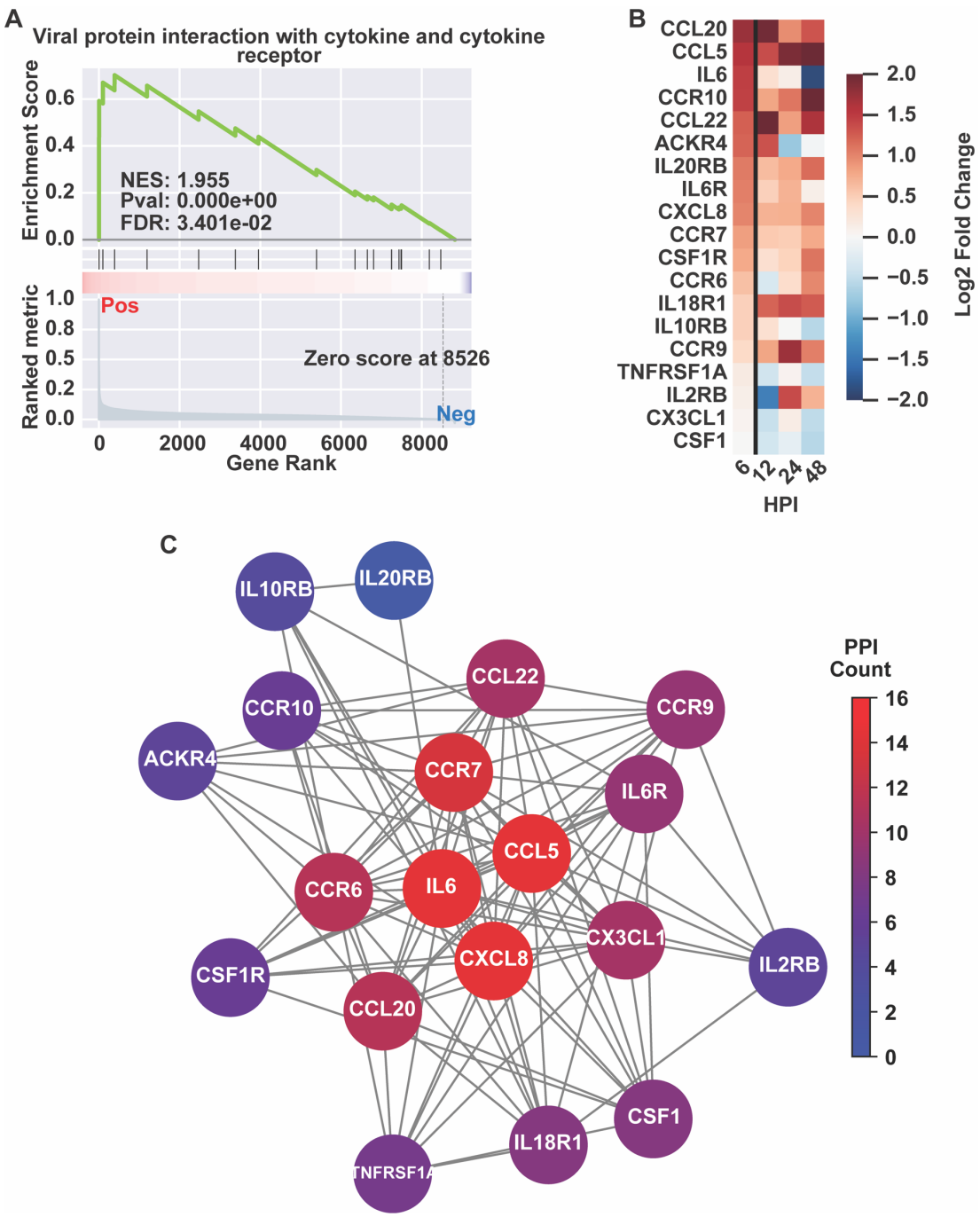

Figure 5. Differential gene expression and network analysis of cytokine-related genes in ZIKV/MR766 vs. PRVABC59. (**A**) Gene set enrichment analysis (GSEA) for "Viral protein interaction with cytokine and cytokine receptor" in ZIKV/MR766 vs. PRVABC59 (upregulated DEGs). The running enrichment score (ES) peaks early, driven primarily by *CCL20*, *CCL5*, *CXCL8*, and *IL6*, with a normalized enrichment score (NES) of 1.955—the highest in this contrast. (**B**) Log_2 fold changes of set genes show upregulation across HPI, with the leading genes among the most highly upregulated. (**C**) Protein-protein interaction (PPI) network from the STRING database, highlighting *CCL5*, *CXCL8*, and *IL6* as key hub genes with extensive connectivity.

DISCUSSION

Our study shows that R06E cells derived from ERBs are susceptible to ZIKV (Figure 1A), whereas the Aji cells derived from the Jamaican fruit bat are not (Figure 1B). The lack of productive replication or transcriptional response to infection suggests that viral replication was not blocked by innate immune responses in the cell. We noted a drop in infectious ZIKV/MR766 recovered from the supernatant at 24 HPI in Aji cells with return to baseline (Figure 1B). We posit that these data suggest possible binding to cellular receptors with reversible adsorption or the virus was endocytosed but failed to uncoat and therefore was not detected by cellular pattern recognition receptors. Our *in vitro* data with a Jamaican fruit bat cell line is incongruous with *in vivo* findings indicating detection of ZIKV antigens in mononuclear cells such as macrophages and microglia of experimentally challenged JFBs, though viremia was not detected in bats from either study(26). It is possible that our immortalized, kidney derived Aji cells with adherent, fibroblast morphology are not a permissive cell type; however, the R06E cells, derived from “the body of an Egyptian rousette bat fetus” are also adherent with fibroblast morphology and do support ZIKV replication. Regardless, our *in vitro* data do not support that JFBs are involved in the sylvatic maintenance of ZIKV in the Americas, consistent with the results of biosurveillance efforts and *in vivo* studies in *Artibeus* spp. bats(22,23,25,30). However, as Reagan *et al*. (1955) reported neurologic disease (described as “nervous symptoms”) in 16 of 20 New World cave bats (*Myotis lucifugus*) inoculated with ZIKV, other bat species may be susceptible to infection with ZIKV in the Americas(31).

R06E cells supported productive replication of both African (ZIKV/MR766) and Asian (ZIKV/PRVABC59) lineage ZIKV isolates (Figure 1A), indicating that ERB-derived cells are permissive to ZIKV infection. Successful replication requires the virus to evade host immune defenses, making viral replication in host cells a key criterion for identifying potential sylvatic reservoirs. Our data with R06E cells aligns with field surveillance efforts reporting detection of ZIKV subgenomic flaviviral RNA (sfRNA) in free-ranging ERBs(4) and low-levels of viremia in experimentally challenged bats(17). Despite efficient ZIKV replication in R06E cells (Figure 1A), the transcriptional immune response did not resemble a well-adapted host-virus relationship (Figure 6). In contrast, ERBs are considered the primary reservoir for the highly pathogenic Marburg virus (MARV), characterized by a controlled inflammatory response to MARV infection(32). *In vitro* experimental work with ERB dendritic cells showed a strong upregulation of type I IFN-related genes with proinflammatory responses downregulated upon infection(33). *In vivo* experiments in ERBs further demonstrated canonical antiviral responses with minimal and organ-specific proinflammatory signaling, notably lacking upregulation of *IL6* and *CCL8*, which are associated with severe disease in humans and nonhuman primates(34,35). The notion of immune tolerance during viral infection through controlled inflammatory response has been widely suggested across several bat-virus systems(36,37), though the extent of this mechanism for tolerating viral infection in bats is unknown(36).

370
371 Although we hypothesized that ERBs might exhibit a tolerant immune response to ZIKV
372 infection, our findings do not align with this expectation. Instead, both African
373 (ZIKV/MR766) and Asian (ZIKV/PRVABC59) isolates triggered robust antiviral and pro-
374 inflammatory responses in R06E cells. Gene set enrichment analysis (GSEA) of R06E
375 cells revealed upregulation of immune-related pathways at 6 HPI, including "viral protein
376 interaction with cytokine and cytokine receptor", "toll-like receptor signaling," and
377 "rheumatoid arthritis" (Fig. 2A, B). These pathways are commonly associated with
378 innate immune activation against viral infections, particularly those driven by interferon-
379 stimulated genes (ISGs). Interestingly, the magnitude of immune response in R06E cells
380 was stronger for ZIKV/MR766 than PRVABC59 (Fig. 2C), suggesting that the African
381 lineage ZIKV strain induces a more robust and earlier antiviral response than the Asian
382 lineage. This is consistent with previous studies reporting higher virulence and immune
383 activation associated with ZIKV/MR766 infections than the Asian ZIKV lineage. Aji cells
384 exhibited no significant enrichment of immune-related gene sets.
385
386 Gene ontology enrichment analysis (GOEA) corroborated our GSEA findings, with
387 R06E cells displaying strong enrichment for immune-related terms (Fig. 3A, B). Among
388 the most significant were "defense response to symbiont," "immune response," and
389 "cytokine-mediated signaling", reinforcing the notion that ZIKV infection in R06E cells
390 activates innate immune pathways. Differentially expressed gene (DEG) clustering
391 revealed three major transcriptional groups in R06E cells. Group 10 genes, including
392 *OAS3*, *MX2*, *IFIT3*, *IFI6*, and *DDX58*, exhibited consistent upregulation across
393 timepoints, confirming their role in ZIKV-driven antiviral defense (Fig. 4A, B). Notably,
394 ZIKV/MR766 induced a stronger response at 6 HPI than ZIKV/PRVABC59, consistent
395 with our GSEA and GOEA findings.
396
397 However, Groups 5 and 8 contained genes with unique expression patterns, being more
398 strongly induced at 6 and 48 HPI in ZIKV/MR766 infections (Fig. 4C, E). These groups
399 were enriched for "GTPase activator activity" and "transmembrane receptor protein
400 tyrosine kinase activity" (Fig. 4D, F), both of which are involved in viral entry, trafficking,
401 and immune signaling. The exact role of these pathways in ZIKV infection remains
402 unclear, but their enrichment suggests potential alternative mechanisms regulating host
403 susceptibility and immune activation. Given the strong enrichment of "viral protein
404 interaction with cytokine and cytokine receptor" in MR766-infected R06E cells, we
405 examined specific genes within this set. GSEA at 6 HPI identified *CCL20*, *CCL5*,
406 *CXCL8*, and *IL6* as among the top upregulated genes (Fig. 5A and 5B). Further, protein-
407 protein interaction (PPI) network analysis identified *CCL5*, *CXCL8*, and *IL6* as major
408 hub genes, suggesting they play central roles in the immune response to ZIKV/MR766
409 infection (Fig. 5C).
410
411 The observed transcriptional responses in ERB cells are consistent with literature on
412 ZIKV infection in other mammals, namely humans and primates, rather than the
413 immune tolerant phenotype observed in ERB cells following infection with MARV(35)

414 (Figure 6). Previous findings from Viet et al. show that flavivirus NS5 proteins—
415 particularly from ZIKV—partially antagonize STAT2-dependent signaling, including in
416 various bat taxa(38). While our transcriptomic analysis of R06E cells revealed robust
417 upregulation of ISGs, including *OAS3*, *MX2*, and *DDX58*, we found that R06E cells
418 supported robust replication of ZIKV. It is possible that degradation of STAT2 in ZIKV-
419 infected R06E cells did dampen interferon signaling, and ISG transcription was driven
420 by alternative STAT-independent pathways (e.g., IRF3/IRF7 activation by RIG-I).
421 Though our current dataset does not allow for mechanistic dissection of these signaling
422 routes, the consistent upregulation of ISGs despite evidence of STAT2 degradation by
423 ZIKV NS5 warrants further investigation into non-canonical interferon signaling in this
424 species.
425
426 ZIKV pathogenicity, disruption of the blood brain barrier, and neuroinflammation are
427 associated with strong induction of chemokines and inflammatory cytokines, of which
428 *IL6* and *CCL5* are key(39,40). Many chemokines, including *CCL5* and *CXCL8*, were
429 found to be upregulated in ZIKV infection experiments as well as in patients with acute
430 infection(41–44). Upregulation of *IL6* is associated with Toll-like receptor activation,
431 leading to heightened inflammation via an NF-κB-favored pathway and subsequent
432 suppression of IFN production, thereby promoting viral replication(45). These findings
433 suggest that despite supporting productive ZIKV replication, ERB cells do not exhibit an
434 immune tolerance phenotype typical of well-adapted viral reservoirs. Instead, the robust
435 proinflammatory response, particularly the strong upregulation of *IL6*, *CCL5*, and
436 *CXCL8*, aligns more closely with a host experiencing acute antiviral activation rather
437 than a long-term reservoir species with a controlled immune response. The observed
438 immune activation could contribute to viral clearance rather than persistent infection,
439 reducing the likelihood that ERBs serve as a primary sylvatic reservoir for ZIKV.
440

441 MATERIALS AND METHODS

442
443 Cell culture and maintenance
444 We grew *Artibeus jamaicensis* immortalized kidney cells (Aji cells), described
445 previously(46) and immortalized *Rousettus aegyptiacus* fetal cell line R06E(47) in
446 Dulbecco's Modified Eagle Medium supplemented with 14% fetal bovine serum (FBS),
447 1% penicillin-streptomycin, 1% L-glutamine, 1% non-essential amino acids (NEAA), and
448 1% sodium pyruvate. We maintained cells at 37°C with 5% CO_2.
449
450 Comparative viral growth curves
451 We conducted viral growth curves using R06E cells and Aji cells by inoculating each cell
452 line at a multiplicity of infection (MOI) of 0.1 with Zika virus (ZIKV) isolates ZIKV/MR766
453 or ZIKV/PRVABC59 in quadruplicate for each time point. We collected supernatant at 0,

454 24, 48, 72, and 96 hours post-inoculation (HPI). We then conducted back titrations to
455 quantify the 50% tissue culture infectious dose ($TCID_{50}$/mL) of the inoculum.
456
457 *In vitro* inoculation for transcriptomics
458 We used two ZIKV isolates in our experiment: MR766 (African lineage, BEI #NR-50065)
459 and PRVABC59 (Asian lineage, BEI #NR-50240). For each virus-cell line combination,
460 we generated three biological replicates and one negative control (PBS-inoculated) in
461 48-well plates. We inoculated all samples at an MOI of 1 and collected samples at five
462 timepoints: 0, 6, 12, 24, and 48 HPI. At each timepoint, we collected infectious virus
463 from the supernatant and scraped TRIzol-inactivated cells from the well surface. We
464 incubated plates for timepoints 6, 12, 24, and 48 HPI at 37 °C with 5% CO_2. We used
465 infectious samples for back titrations and processed inactivated cells for RNA
466 sequencing (RNA-seq).
467
468 We extracted RNA from TRIzol-inactivated R06E cells using either TRIzol™ (Invitrogen)
469 for manual phase separation or the Direct-zol™ 96 RNA extraction kit (Zymo) following
470 the manufacturer's instructions. We prepared total RNA-seq libraries using the Zymo-
471 Seq RiboFree® Total RNA Library Kit (Zymo Research), performed fragment analysis
472 for quality control, and sequenced libraries on an Illumina NextSeq 2000 as paired-end
473 reads (2×100 bp). Samples were meant to have 3 biological replicates, but due to low
474 quality and other technical issues, many replicates were removed. Most samples
475 maintained 2-3 replicates, but 3 samples ended with only 1 replicate: 2 of the Aji
476 samples and 1 of the R06E samples. Supplemental Table 2 has the complete replicate
477 counts, with column 1 listing "{cell line}-{virus treatment}-{timepoint}" in this format, and
478 column 2 listing the counts.
479
480 RNA-seq Read Processing and Mapping
481 RNA sequencing reads were first processed by running them through the fastp tool(48),
482 with adapter removal (see code for command). The trimmed reads underwent QC by
483 subsequently running them through FastQC
484 (http://www.bioinformatics.babraham.ac.uk/projects/fastqc/) and the output graphs were
485 manually inspected. All samples appeared acceptable at this step.
486
487 Reads were then mapped to their respective genomes with corresponding annotations
488 from NCBI. For *Rousettus* the GCF_014176215.1_mRouAeg1.p_genomic genome(49)
489 and annotations were used, and for *Artibeus* the
490 GCF_021234435.1_CSHL_Jam_final_genomic genome(50) and annotations were
491 used. The mapping tool STAR(51) was used to build genome indices from the
492 respective genome and annotation files. Consequently, when STAR mapping was
493 performed it was able to provide gene counts concurrently with read mapping, removing
494 the need for an additional gene counting step.
495
496 Gene Count Processing, Batch Correction, and Normalization

Several steps were carried out for initial gene count processing. First, 6 samples had technical replicates, so the resulting gene counts were combined within technical replicates. Next, manual inspection revealed 2 samples exhibited huge proportions of missing or skewed genes, so these were removed from subsequent analyses. Lastly, the gene counts were collated into a single table. These steps were facilitated by the gene_count_and_metadata_processing.py script.

The batch effect of RNA-seq library preparation was then corrected using pyComBat(52). Since pyComBat builds a comprehensive model to quantify and remove batch effect, we chose to process gene counts by cell line to reduce runtime and computational load. However, within each cell line we did demarcate virus treatment and timepoints as covariates in pyComBat so their effects would not be lost during correction.

Finally, gene counts were normalized using PyDESeq2(53). The resulting normalized gene counts are returned in the code as a python object, by which several analyses may be performed, including differentially expressed gene (DEG) identification and principal component analysis. However, for DEG identification and p-value calculations, the current PyDESeq2 module lacks granularity for multifactor models. For instance, it can calculate DEGs with p-values between virus treatment contrasts (e.g. no treatment vs MR766 treatment) or timepoint contrasts (e.g. 6 HPI vs 12 HPI), but not both (e.g 6 HPI no treatment vs 6 HPI MR766 treatment). Consequently, depending on the analysis we performed, the data was parsed to the necessary level of granularity before normalization. This is specified below, per analysis.

Principal Component Analysis

For the principal component analysis (PCA), gene counts were parsed by cell line and virus treatment contrast, then normalized with PyDESeq2. The resulting counts underwent PCA using the scanpy module(54).

Spearman Correlations

For Spearman correlations, the gene counts were parsed only by cell line, then normalized with PyDESeq2. The mean gene count values were calculated for replicates, and then any genes with a mean count of 0 for all samples were dropped to prevent artificially inflating the correlation due to genes that may simply not be expressed in the cell lines. Finally, the curated gene count means were used for pairwise Spearman correlations. The coefficients were rounded to 4 significant figures and plotted.

Differentially Expressed Gene Identification

To appropriately calculate DEG $\log_2$ fold changes and p-values in our multifactor design, the gene counts were parsed by cell line, virus treatment contrasts, and then timepoint, and the subsets normalized with PyDESeq2 (e.g. ‘R06E 6 HPI no treatment’ vs ‘R06E 6 HPI MR766 treatment’. Then, using the PyDESeq2 DeseqStats() function,

541 $\log_2$ fold changes and Wald test p-values were calculated. These p-values are adjusted
542 for multiple hypotheses. Depending on the analysis, the DEGs were filtered by $\log_2$ fold
543 change and p-value, as stated below.
544
545 Gene Set Enrichment Analysis
546 The $\log_2$ fold changes and p-values previously calculated were used for gene set
547 enrichment analysis (GSEA) without filtering for non-DEGs (i.e. all genes were used).
548 All genes were ranked, per gene, using the equation:
549
550 $$\text{rank} = -\log_{10}(\text{p-value}) * \log_2 \text{ fold change}$$
551
552 Thus, both the fold change and the p-value informed how enriched a gene was amongst
553 all genes. However, because a gene set is not necessarily a pathway, and at times may
554 exhibit both up and down expression, we chose to perform GSEA separately for up and
555 down regulated genes. When analyzing downregulated genes, we multiplied the $\log_2$
556 fold change by negative 1 to make the resulting enrichment scores positive. Lastly, the
557 ranked genes were scaled by dividing all rank values by the max value, thus making the
558 new scaled max value always 1. This had no effect on the order of genes or the
559 enrichment statistics; it was primarily done to make direct comparison of rank across
560 virus contrasts more intuitive (e.g. the scaled ranks can be seen in Figure 5A, running
561 from 1 to 0).
562
563 The ranked genes were then used as input for the GSEApy module (55), which
564 calculated normalized enrichment scores (NESs) and false discovery rates (FDRs) per
565 gene set. We used the KEGG_2021_Human gene sets (56), as there were no defined
566 KEGG bat gene sets for the module (though there may be elsewhere) and bats are not
567 a model organism, whereas the human genome is well characterized, and the human
568 gene sets well-curated. Enriched gene sets were calculated for all contrasts and
569 timepoints, but we chose to highlight only the top 10 gene sets with the lowest FDRs for
570 6 HPI (per virus contrast) and subsequently depict the NESs for these gene sets across
571 all time points (Figure 2).
572
573 Gene Ontology Enrichment Analysis
574 The DEGs were filtered for gene ontology enrichment analysis (GOEA) by selecting
575 genes with an absolute $\log_2$ fold change greater than 1.5 and p-value of less than 0.05.
576 The remaining genes were used as input for the goatools python module (57) to perform
577 GOEA. The GO term tree was built using the main go.obo file from the
578 geneontology.org website (see code for ftp path) and DEG IDs were mapped to GO
579 terms using the gene2go.txt file from the NCBI (see code for ftp path) and taxon ID
580 9407. Lastly, a file containing all *Rousettus* genes was acquired from the NCBI using
581 the search query:
582
583 "9407"[Taxonomy ID] AND alive[property] AND genetype protein coding[Properties]
584

585 This file was used by goatools as the baseline “background genes” set for determining
586 which GO terms were biologically enriched and not enriched by chance.
587
588 The enriched GO term results from the primary GOEA were then mapped to the GO
589 slim terms in the goslim_pir.obo file from the geneontology.org website. This allowed us
590 to group enriched GO terms and reduce redundancy; however, the GO slim terms
591 (representing subsets of the full ontology) tend to be broad and high-level. For our
592 analyses and interpretation, we took the GO term with the most significant p-value in
593 each GO slim group and chose that to represent the entire group (see Supplemental
594 Figure 2). In most cases, the most enriched term was not the GO slim term, but in the
595 rare cases it was, we chose the second most enriched term to increase interpretability.
596 These are the GO terms used in the paper and figures.
597
598 DEG Expression Pattern Identification
599 As per the GOEA, DEGs were filtered so remaining genes had an absolute $\log_2$ fold
600 change greater than 1.5 and p-value of less than 0.05. The counts for these genes were
601 then clustered by the R package DEGreport (58); more specifically, the degPatterns()
602 function. Default parameters were used, including a minimum count of 15 genes per
603 group for a group to be reported and a clustering coefficient cutoff of 0.7. Consequently,
604 only 3 viable groups were generated, as shown in Figure 4.
605
606 Protein-Protein Interaction Network Analysis
607 The 6 HPI upregulated genes (see Fig 5B) in the KEGG “Viral Protein Interaction With
608 Cytokine and Cytokine Receptor” gene set were submitted to the STRING database
609 version 12.0(29) via the STRING API with default parameters. The API request returned
610 a list of gene interactions with scores representing the likelihood of interaction based on
611 different factors such as literature sources describing interaction. The interactions were
612 used to generate a protein-protein interaction (PPI) network, where the edges were
613 interactions between genes and the weights of the edges were the interaction scores
614 pulled from the database. The genes were examined for interaction counts (i.e. number
615 of edges) and the genes with the highest counts were identified as hub genes; the most
616 interconnected genes of the network which play potentially central roles. The interaction
617 count was also depicted graphically (Fig 5C). The network was generated using the
618 NetworkX module(59) and the Fruchterman-Reingold force-directed algorithm
619 (encapsulated in the spring_layout() function).
620
621 **Data Analysis and Visualization**
622 The bioinformatic analyses were performed or orchestrated by in-house code, which
623 can be found in the GitHub repo below. Additionally, they were run in a Singularity
624 container made from a Docker image. While the Docker image is not publicly available,
625 the build file for building the image is in the same repo.
626
627 The graphs and other data visualizations presented in the paper were either generated
628 using the modules for each respective analysis (e.g. GSEApy), or the same previously

mentioned in-house code, leveraging Matplotlib (60) and seaborn (61). The code to reproduce the analyses and visualization is available through GitHub (https://github.com/viralemergence/zika-rnaseq-analysis). Lastly, the figure labels were re-generated with Adobe Illustrator to increase readability, and the figures were exported from Illustrator to make high resolution files.

Biosafety Statement

All experimental work with Zika virus was conducted under elevated biosafety laboratory practices at Washington State University as approved by the Institutional Biosafety Committee.

Data Availability

Illumina reads are available from the sequencing read archive (SRA, accession: PRJNA1241890).

ACKNOWLEDGEMENTS

This research was supported by funding to Verena (viralemergence.org) from the U.S. National Science Foundation grant number NSF DBI 2515340. ACF was supported by the National Institutes of Health grant number K01OD037645. The following reagents were obtained through BEI Resources, NIAID, NIH, as part of the WRCEVA program: Zika Virus, MR 766, NR-50065; Zika Virus, PRVABC59; R06E, *Rousettus aegyptiacus* (Egyptian fruit bat), Immortalized Fetal Cell Line, NR-49168. We thank Dr. Tony Schountz for sharing *Artibeus jamaicensis* primary cells which we immortalized prior to this study. We thank Dr. Jiwen Qiu for his assistance with RNA extractions for this study. This research used resources of the Center for Institutional Research Computing at Washington State University.

AUTHOR CONTRIBUTIONS

SNS, ACF, AJB, and ES conceptualized the project. SNS, AJB, JG, and JH completed data curation and formal analysis. SNS, RR, MK, and ML provided resources and refined the methodology. SNS and ACF managed and supervised the project and acquired funding. SNS, AJB, JG, and ACF drafted the original manuscript and, along with JH, RR, MK, ML, and ES, reviewed and edited the manuscript.

REFERENCES

1. Barreto de Araújo TV, Ximenes RAA, Miranda-Filho DB, Souza WV, Montarroyos UR, Melo APL, et al. Association between microcephaly, Zika virus infection and other risk factors in Brazil, final report of a case-control study. Lancet Infect Dis. 2018 Mar 1;18(3):328–36.

2. Krauer F, Riesen M, Reveiz L, Oladapo OT, Martínez-Vega R, Porgo TV, et al. Zika Virus Infection as a Cause of Congenital Brain Abnormalities and Guillain–Barré Syndrome: Systematic Review. PLoS Med. 2017 Jan 3;14(1):e1002203.

3. Musso D, Ko AI, Baud D. Zika Virus Infection — After the Pandemic. New England Journal of Medicine. 2019 Oct 10;381(15):1444–57.

4. Fagre AC, Lewis J, Miller MR, Mossel EC, Lutwama JJ, Nyakarahuka L, et al. Subgenomic flavivirus RNA (sfRNA) associated with Asian lineage Zika virus identified in three species of Ugandan bats (family Pteropodidae). Sci Rep. 2021 Apr 16;11:8370.

5. Faria NR, Azevedo R do S da S, Kraemer MUG, Souza R, Cunha MS, Hill SC, et al. Zika virus in the Americas: Early epidemiological and genetic findings. Science. 2016 Apr 15;352(6283):345–9.

6. World Health Organization [Internet]. 2016 [cited 2024 Dec 18]. The history of zika virus. Available from: https://www.who.int/news-room/feature-stories/detail/the-history-of-zika-virus

7. de Oliveira FBC, Freire VPAS de S, Coelho SVA, Meuren LM, Palmeira J da F, Cardoso AL, et al. ZIKV Strains Elicit Different Inflammatory and Anti-Viral Responses in Microglia Cells. Viruses. 2023 May 26;15(6):1250.

8. Dowall SD, Graham VA, Rayner E, Hunter L, Atkinson B, Pearson G, et al. Lineage-dependent differences in the disease progression of Zika virus infection in type-I interferon receptor knockout (A129) mice. PLOS Neglected Tropical Diseases. 2017 Jul 3;11(7):e0005704.

9. Shao Q, Herrlinger S, Zhu YN, Yang M, Goodfellow F, Stice SL, et al. The African Zika virus MR-766 is more virulent and causes more severe brain damage than current Asian lineage and dengue virus. Development. 2017 Nov 15;144(22):4114–24.

10. Simonin Y, van Riel D, van de Perre P, Rockx B, Salinas S. Differential virulence between Asian and African lineages of Zika virus. PLoS Neglected Tropical Diseases. 2017;11(9):e0005821.

11. Abreu FVS de, Ferreira-de-Brito A, Azevedo A de S, Linhares JHR, de Oliveira Santos V, Hime Miranda E, et al. Survey on Non-Human Primates and Mosquitoes Does not Provide Evidences of Spillover/Spillback between the Urban and Sylvatic Cycles of Yellow Fever and Zika Viruses Following Severe Outbreaks in Southeast Brazil. Viruses. 2020 Mar 26;12(4):364.

12. Althouse BM, Vasilakis N, Sall AA, Diallo M, Weaver SC, Hanley KA. Potential for Zika Virus to Establish a Sylvatic Transmission Cycle in the Americas. PLoS Negl Trop Dis. 2016 Dec 15;10(12):e0005055.

13. Berry N, Ferguson D, Ham C, Hall J, Jenkins A, Giles E, et al. High susceptibility, viral dynamics and persistence of South American Zika virus in New World monkey species. Sci Rep. 2019 Oct 10;9(1):14495.

14. Zhou H, Eaton B, Hu Z, Arif B. Accidental discovery and isolation of Zika virus in Uganda and the relentless epidemiologist behind the investigations. Virol Sin. 2016 Jul 18;31(4):357–61.

15. Crabtree MB, Kading RC, Mutebi JP, Lutwama JJ, Miller BR. Identification of host blood from engorged mosquitoes collected in western uganda using cytochrome oxidase i gene sequences. Journal of Wildlife Diseases. 2013 Jul 1;49(3):611–26.

16. Shepherd R, Williams M. Studies on viruses in East African bats (Chiroptera). 1. Haemagglutination inhibition and circulation of arboviruses. Zoonoses research. 1964;3(3):125–39.

17. Simpson DIH, O'Sullivan JP. Studies on arboviruses and bats (Chiroptera) in East Africa. Annals of Tropical Medicine & Parasitology [Internet]. 1968 Dec 1 [cited 2025 Jan 24]; Available from: https://www.tandfonline.com/doi/abs/10.1080/00034983.1968.11686579

18. Kumm HW. Yellow Fever Transmission Experiments with South American Bats. Annals of Tropical Medicine & Parasitology [Internet]. 1932 Jul 14 [cited 2024 Dec 19]; Available from: https://www.tandfonline.com/doi/abs/10.1080/00034983.1932.11684716

19. Kading RC, Schountz T. Flavivirus Infections of Bats: Potential Role in Zika Virus Ecology. Am J Trop Med Hyg. 2016 Nov 2;95(5):993–6.

20. Simpson D, Williams M, O'Sullivan J, Cunningham J, Mutere F. Studies on arboviruses and bats (Chiroptera) in East Africa: II.—Isolation and haemagglutination-inhibition studies on bats collected in Kenya and throughout Uganda. Annals of Tropical Medicine & Parasitology. 1968;62(4):432–40.

21. Espinoza-Gómez A, Moreno-Santillán DD, Juárez-Maldonado R, Gutiérrez EG, Salazar MI, Alonso-Palomares LA, et al. Identification of viral RNA sequences in vampire bats (Desmodus rotundus) from central Mexico. Revista mexicana de biodiversidad

[Internet]. 2022 [cited 2025 Jan 20];93. Available from: http://www.scielo.org.mx/scielo.php?script=sci_abstract&pid=S1870-34532022000100318&lng=es&nrm=iso&tlng=en

22. Torres-Castro M, Noh-Pech H, Hernández-Betancourt S, Peláez-Sánchez R, Lugo-Caballero C, Puerto FI. West Nile and Zika viruses in bats from a suburban area of Merida, Yucatan, Mexico. Zoonoses Public Health. 2021 Apr 20;

23. Hernández-Aguilar I, Lorenzo C, Ramírez-Palacios LR, Santos-Moreno A, Naranjo EJ. Molecular Detection of Dengue Virus, Zika Virus, and Chikungunya Virus Arboviruses in Neotropical Bats. Vector-Borne and Zoonotic Diseases. 2023 Aug;23(8):428–36.

24. Aguilar-Setién A, Salas-Rojas M, Gálvez-Romero G, Almazán-Marín C, Moreira-Soto A, Alfonso-Toledo J, et al. Experimental infection of Artibeus lituratus bats and no detection of Zika virus in neotropical bats from French Guiana, Peru, and Costa Rica suggests a limited role of bats in Zika transmission. PLOS Neglected Tropical Diseases. 2023 Jul 24;17(7):e0010439.

25. Bittar C, Machado RRG, Comelis MT, Bueno LM, Morielle-Versute E, Beguelini MR, et al. Lack of serological and molecular evidence of arbovirus infections in bats from Brazil. PLOS ONE. 2018 Nov 7;13(11):e0207010.

26. Malmlov A, Bantle C, Aboellail T, Wagner K, Campbell CL, Eckley M, et al. Experimental Zika virus infection of Jamaican fruit bats (Artibeus jamaicensis) and possible entry of virus into brain via activated microglial cells. PLOS Neglected Tropical Diseases. 2019 Feb 4;13(2):e0007071.

27. Luu AP, Yao Z, Ramachandran S, Azzopardi SA, Miles LA, Schneider WM, et al. A CRISPR Activation Screen Identifies an Atypical Rho GTPase That Enhances Zika Viral Entry. Viruses. 2021 Nov;13(11):2113.

28. Kim JH, Koh B, Ahn DG, Lee SJ, Park TJ, Park JP. A screening study of high affinity peptide as molecular binder for AXL, tyrosine kinase receptor involving in Zika virus entry. Bioelectrochemistry. 2021 Feb 1;137:107670.

29. Szklarczyk D, Kirsch R, Koutrouli M, Nastou K, Mehryary F, Hachilif R, et al. The STRING database in 2023: protein–protein association networks and functional enrichment analyses for any sequenced genome of interest. Nucleic Acids Research. 2023 Jan 6;51(D1):D638–46.

30. Aguilar-Setién A, Salas-Rojas M, Gálvez-Romero G, Almazán-Marín C, Moreira-Soto A, Alfonso-Toledo J, et al. Experimental infection of Artibeus lituratus bats and no detection of Zika virus in neotropical bats from French Guiana, Peru, and Costa Rica suggests a limited role of bats in Zika transmission. PLOS Neglected Tropical Diseases. 2023 Jul 24;17(7):e0010439.

31. Reagan RL, Rumbaugh H, Nelson H, Brueckner AL. Effect of Zika Virus and Bwamba Virus in the Cave Bat (Myotus lucifugus). Transactions of the American Microscopical Society. 1955;74(1):77–9.

32. Towner JS, Amman BR, Sealy TK, Carroll SAR, Comer JA, Kemp A, et al. Isolation of genetically diverse Marburg viruses from Egyptian fruit bats. PLoS Pathog. 2009 Jul;5(7):e1000536.

33. Prescott J, Guito JC, Spengler JR, Arnold CE, Schuh AJ, Amman BR, et al. Rousette Bat Dendritic Cells Overcome Marburg Virus-Mediated Antiviral Responses by Upregulation of Interferon-Related Genes While Downregulating Proinflammatory Disease Mediators. mSphere. 2019 Dec 4;4(6):e00728-19.

34. Guito JC, Prescott JB, Arnold CE, Amman BR, Schuh AJ, Spengler JR, et al. Asymptomatic Infection of Marburg Virus Reservoir Bats Is Explained by a Strategy of Immunoprotective Disease Tolerance. Current Biology. 2021 Jan 25;31(2):257-270.e5.

35. Guito JC, Kirejczyk SGM, Schuh AJ, Amman BR, Sealy TK, Graziano J, et al. Coordinated inflammatory responses dictate Marburg virus control by reservoir bats. Nat Commun. 2024 Feb 28;15(1):1826.

36. Letko M, Seifert SN, Olival KJ, Plowright RK, Munster VJ. Bat-borne virus diversity, spillover and emergence. Nat Rev Microbiol. 2020 Aug;18(8):461–71.

37. Schountz T, Baker ML, Butler J, Munster V. Immunological Control of Viral Infections in Bats and the Emergence of Viruses Highly Pathogenic to Humans. Front Immunol [Internet]. 2017 Sep 11 [cited 2025 Feb 20];8. Available from: https://www.frontiersin.org/journals/immunology/articles/10.3389/fimmu.2017.01098/full

38. Veit EC, Salim MS, Jung MJ, Richardson RB, Boys IN, Quinlan M, et al. Evolution of STAT2 resistance to flavivirus NS5 occurred multiple times despite genetic constraints. Nat Commun. 2024 Jun 26;15(1):5426.

39. Metzler AD, Tang H. Zika Virus Neuropathogenesis—Research and Understanding. Pathogens. 2024 Jul;13(7):555.

40. Magoro T, Dandekar A, Jennelle LT, Bajaj R, Lipkowitz G, Angelucci AR, et al. IL-1β/TNF-α/IL-6 inflammatory cytokines promote STAT1-dependent induction of CH25H in Zika virus-infected human macrophages. J Biol Chem. 2019 Oct 4;294(40):14591–602.

41. Michlmayr D, Lim JK. Chemokine receptors as important regulators of pathogenesis during arboviral encephalitis. Front Cell Neurosci [Internet]. 2014 Sep 30 [cited 2025 Jan 22];8. Available from: https://www.frontiersin.org/journals/cellular-neuroscience/articles/10.3389/fncel.2014.00264/full

42. Chen Q, Li N, Zeng S, Wu S, Luo X, Zhang S, et al. ZIKV infection differentially affects the transcriptional profiles in HTR8 and U251 cells. Virus Research. 2023 Sep 1;334:199166.

43. Naveca FG, Pontes GS, Chang AY hen, Silva GAV da, Nascimento VA do, Monteiro DC da S, et al. Analysis of the immunological biomarker profile during acute Zika virus infection reveals the overexpression of CXCL10, a chemokine linked to neuronal damage. Mem Inst Oswaldo Cruz. 2018 May 14;113:e170542.

44. Mladinich MC, Conde JN, Schutt WR, Sohn SY, Mackow ER. Blockade of Autocrine CCL5 Responses Inhibits Zika Virus Persistence and Spread in Human Brain Microvascular Endothelial Cells. mBio. 2021 Aug 31;12(4):e0196221.

45. Plociennikowska A, Frankish J, Moraes T, Del Prete D, Kahnt F, Acuna C, et al. TLR3 activation by Zika virus stimulates inflammatory cytokine production which dampens the antiviral response induced by RIG-I-like receptors. J Virol. 2021 Apr 26;95(10):e01050-20, JVI.01050-20.

46. Letko M, Marzi A, Munster V. Functional assessment of cell entry and receptor usage for SARS-CoV-2 and other lineage B betacoronaviruses. Nat Microbiol. 2020 Apr;5(4):562–9.

47. Jordan I, Munster VJ, Sandig V. Authentication of the R06E Fruit Bat Cell Line. Viruses. 2012 May;4(5):889–900.

48. Chen S, Zhou Y, Chen Y, Gu J. fastp: an ultra-fast all-in-one FASTQ preprocessor. Bioinformatics. 2018 Sep 1;34(17):i884–90.

49. Jebb D, Huang Z, Pippel M, Hughes GM, Lavrichenko K, Devanna P, et al. Six reference-quality genomes reveal evolution of bat adaptations. Nature. 2020 Jul;583(7817):578–84.

50. Pumo DE, Finamore PS, Franek WR, Phillips CJ, Tarzami S, Balzarano D. Complete mitochondrial genome of a neotropical fruit bat, Artibeus jamaicensis, and a new hypothesis of the relationships of bats to other eutherian mammals. J Mol Evol. 1998 Dec;47(6):709–17.

51. Dobin A, Gingeras TR. Mapping RNA-seq Reads with STAR. CP in Bioinformatics [Internet]. 2015 Sep [cited 2025 Jan 14];51(1). Available from: https://currentprotocols.onlinelibrary.wiley.com/doi/10.1002/0471250953.bi1114s51

52. Behdenna A, Colange M, Haziza J, Gema A, Appé G, Azencott CA, et al. pyComBat, a Python tool for batch effects correction in high-throughput molecular data using empirical Bayes methods. BMC Bioinformatics. 2023 Dec 7;24(1):459.

53. Muzellec B, Teleńczuk M, Cabeli V, Andreux M. PyDESeq2: a python package for bulk RNA-seq differential expression analysis. Ponty Y, editor. Bioinformatics. 2023 Sep 2;39(9):btad547.

54. Wolf FA, Angerer P, Theis FJ. SCANPY: large-scale single-cell gene expression data analysis. Genome Biol. 2018 Dec;19(1):15.

55. Fang Z, Liu X, Peltz G. GSEApy: a comprehensive package for performing gene set enrichment analysis in Python. Lu Z, editor. Bioinformatics. 2023 Jan 1;39(1):btac757.

56. Kanehisa M. KEGG: Kyoto Encyclopedia of Genes and Genomes. Nucleic Acids Research. 2000 Jan 1;28(1):27–30.

57. Klopfenstein DV, Zhang L, Pedersen BS, Ramírez F, Warwick Vesztrocy A, Naldi A, et al. GOATOOLS: A Python library for Gene Ontology analyses. Sci Rep. 2018 Jul 18;8(1):10872.

58. Lorena Pantano [Aut C. DEGreport [Internet]. Bioconductor; 2017 [cited 2025 Jan 15]. Available from: https://bioconductor.org/packages/DEGreport

59. Hagberg A, Schult D, Swart P. Exploring network structure, dynamics, and function using NetworkX. Proceedings of the 7th Python in Science Conference (SciPy2008). 2008 Aug;11–5.

60. Hunter JD. Matplotlib: A 2D Graphics Environment. Comput Sci Eng. 2007;9(3):90–5.

61. Waskom M. seaborn: statistical data visualization. JOSS. 2021 Apr 6;6(60):3021.